Macromolecules

ARTICLE

pubs.acs.org/Macromolecules

Time-Domain NMR Observation of Entangled Polymer Dynamics: Analytical Theory of Signal Functions

Fabián Vaca Chávez*,† and Kay Saalwächter*

Institut für Physik — NMR, Martin-Luther-Universität Halle-Wittenberg, Betty-Heimann-Str. 7, D-06120 Halle, Germany

ABSTRACT: We present a full analytical treatment of signal functions in time-domain NMR of entangled polymer melts. Our approach is based on the segmental orientation autocorrelation function for entangled chains previously determined experimentally via field cycling NMR, on the one hand, and via analyzing the initial rise of normalized double-quantum buildup curves, on the other hand, which yield consistent data over about 10 decades in time based on time−temperature superposition. The correlation function is similar to but deviates in a few aspects from the predictions of the tube model. We use the Anderson−Weiss approximation to derive formulas for different signal functions for simple transverse relaxation experiments and specifically for the signal functions from multiple-quantum NMR. We demonstrate that our treatment is, for moderate NMR evolution times, in good agreement with proton NMR data of entangled poly(butadiene) samples over large temperature and molecular weight ranges. Our results represent a showcase for the applicability of the Anderson−Weiss approximation for the calculation of transverse relaxation phenomena of entangled polymers. Open questions concern the exact form of the autocorrelation function at very short times, where it reflects the local (glassy) dynamics.

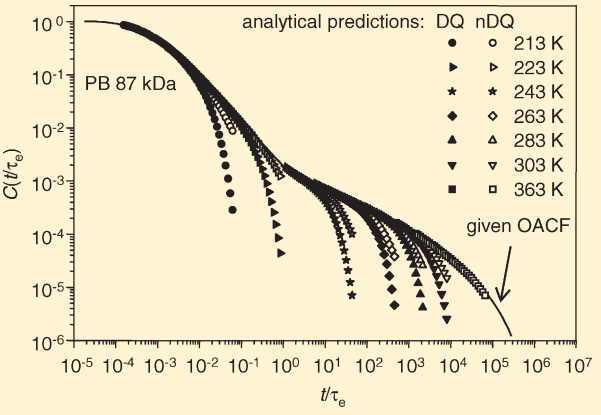

I. INTRODUCTION

Since de Gennes presented the reptation model almost 40 years ago,[1] the experimental study of polymer dynamics and its theoretical understanding has been an active focus of polymer physics. The reptation model describes the motion of an entangled polymer chain through a net of immobile obstacles representing the other polymer chains, creating a "tube" which the chain is confined to. A combination with the Rouse theory for unentangled chains[2] resulted in what is today referred to as the tube model of polymer dynamics.[3] This model describes entangled melt rheology qualitatively well, yet the improvements—or the necessity for an entirely new theoretical approach—needed to achieve a truly quantitative understanding are a matter of active debate.[4] While the melt rheology, ideally in the form of mechanical spectroscopy, stands at the very heart of any serious endeavor to understand polymer melt properties,[5] the understanding of the data requires the use of theoretical models. In turn, actual, critical tests of model ingredients are the domain of molecular techniques, where dielectric spectroscopy[6] and scattering techniques[7] stand out in that they have entered the realm of textbook knowledge.[8]

NMR, while offering a rich toolbox of multiple techniques to study polymer structure and dynamics,[9,10] is not yet on par with its competitors as to its reception in the polymer physics community, mainly owing to its utter complexity. We here hope to improve on this aspect, stressing the use of a simple segmental orientation autocorrelation function (OACF) as a descriptor of polymer dynamics

$$C(t) = \langle P_2(\cos\theta(t))P_2(\cos\theta(0))\rangle \quad (1)$$

This function provides a sufficiently accurate description in many seemingly complex circumstances once fast local dynamics is uniaxially symmetric, which is the case for any polymer already on the level of conformational jumps within individual segments at temperatures that are sufficiently far above T_g. On the one hand, correlation functions such as $C(t)$ can be easily treated theoretically or deduced from computer simulations.[11,12] On the other hand, $C(t)$ can be obtained from NMR[13−17] and/or can be used to compute the NMR response of a mobile polymer, which is the subject of this work. Finally, as also discussed in our preceding paper,[17] it directly reflects rheological properties, as it describes local conformational order related to entropic elasticity. It is no coincidence that the $C(t)$ for an entangled melt sketched in Figure 1 resembles the behavior of the stress relaxation modulus.

It is well-known that NMR provides a vast number of experimental techniques to study polymer dynamics. We here focus on time-domain techniques based on coherent spin evolution and transverse relaxation phenomena under multiple dipole−dipole couplings, as found in simple proton NMR;

Received: November 11, 2010
Revised: January 25, 2011
Published: February 28, 2011

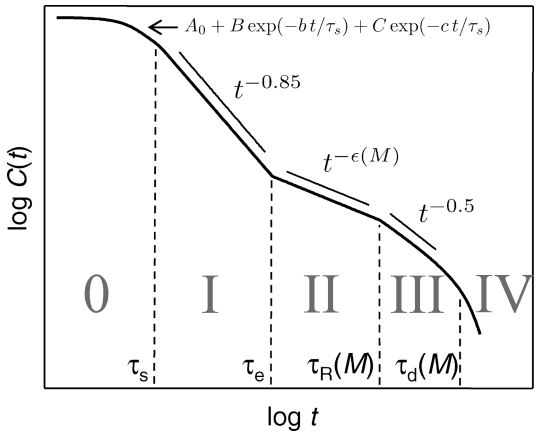

Figure 1. Schematic segmental orientation autocorrelation function for an entangled polymer melt, as obtained from experiments on poly(butadiene). In previous work,[13,14,16,17] it was shown that this function is in principle compatible with the Doi−Edwards regimes 0−IV of the tube model (regime 0 representing glassy dynamics); however, the regime I and regime II power-law exponents deviate from the predictions of −1 and −1/4, respectively. Regime transitions occur at the segmental (τ_s), entanglement (τ_e), Rouse (τ_R), and disentanglement (τ_d) times.

however, we emphasize that the formalism is equally applicable for quadrupolar ^{2}H NMR. For entangled polymer melts far above T_g, such NMR techniques make use of residual anisotropic spin interactions which arise from anisotropic segmental fluctuations due to the existence of topological constraints, and $C(t)$ quantitatively reflects the time-averaged degree of this anisotropy up to the given time. While simple T_2 relaxometry is undoubtedly the most popular representative of this class of techniques, we concentrate on proton multiple quantum (MQ) NMR, which has evolved as a powerful tool with a number of advantages.[18]

Our starting point is the $C(t)$ for an entangled melt shown in Figure 1, which was experimentally determined via a combination of field-cycling T_1 relaxometry[13] and proton MQ NMR,[14,16,17] both relying on time−temperature superposition to obtain data over about 10 decades in time and the latter having been used only approximately in the short-time initial-rise regime. We refer the reader to these previous publications concerning the interpretation of $C(t)$ with regards to the (limited) applicability of the tube model and the conclusions thereof.

We follow closely the important work of Ball, Callaghan, and Samulski (BCS), who have used the same theoretical framework, namely a second-moment (Anderson−Weiss, AW) approximation,[19] to calculate the Hahn echo decay and the so-called β echo for elastomers[20] and entangled melts.[21,22] Their method, being quite analogous to MQ NMR in certain respects, as well as their underlying model for $C(t)$ had a few shortcomings, which we here remedy, arriving at predictions for the different time-domain signals, which fit MQ and T_2 NMR data very well over a large temperature and molecular-weight range, subject to the limitation that second-moment approximations cannot describe data at long evolution times. On the basis of the full analytical treatment, we critically discuss the applicability limits of the initial-rise analysis of MQ data that was the basis of previous work.[14−17] We end with an overview and a critical discussion of earlier NMR work on polymer melts and elastomers.

II. METHODOLOGICAL AND THEORETICAL BACKGROUND

The proton MQ NMR experiment referred to in this work is addressed in much detail in ref 18. It basically consists of an excitation period (τ_{exc}) and a reconversion period (τ_{rec}) during which a specific pulse sequence is applied[23] and simple intensity detection after a 90° pulse. The durations of the first two periods are equal $\tau_{exc} = \tau_{rec} = \tau_{DQ}$. During the pulse sequence, the spin system evolves under a pure double-quantum (DQ) Hamiltonian

$$\bar{H}_{DQ} = -\frac{a(\psi)}{2}\sum_{i<j} D_{eff}^{ij} P_2(\cos\beta)(\hat{I}_+^i \hat{I}_+^j + \hat{I}_-^i \hat{I}_-^j) \quad (2)$$

where $P_2(x)$ is the second Legendre polynomial, $\hat{I}_{+,-}$ are spin operators, and $a(\psi) \leq 1.0$ is a scaling factor taking into account finite-pulse effects; it is always absorbed into and thus used to correct the effective time argument τ_{DQ}. Equation 2 represents an approximation in that only spin pairs $\{i, j\}$ within a statistical segment are considered. D_{eff}^{ij} are thus effective dipole−dipole coupling constants that arise from a preaveraging by fast intrasegmental motions. The corresponding dipole−dipole coupling tensors are in this limit collinear; thus, β can be taken as the angle between the polymer backbone and the external (static) magnetic field $\mathbf{B}_0$. This approximative view will of course break down at temperatures below which intrasegmental motions are not fast as compared to the inverse static line width, i.e., in regime 0 or slightly beyond.

The sequence excites all even quantum orders, and using appropriate phase cycling, the pulse sequence produces either a buildup signal dominated by DQ coherences (I_{DQ}) or a reference (I_{ref}), from which a fully dipolar-refocused sum signal ($I_{\Sigma MQ}$) can be constructed:

$$I_{DQ} = \langle \sin\phi_1 \sin\phi_2 \rangle \simeq \sinh\langle\phi_1\phi_2\rangle e^{-\langle\phi_1^2\rangle} \quad (3)$$

$$I_{ref} = \langle \cos\phi_1 \cos\phi_2 \rangle \simeq \cosh\langle\phi_1\phi_2\rangle e^{-\langle\phi_1^2\rangle} \quad (4)$$

$$I_{\Sigma MQ} = \langle \sin\phi_1 \sin\phi_2 \rangle + \langle \cos\phi_1 \cos\phi_2 \rangle \simeq e^{\langle\phi_1\phi_2\rangle} e^{-\langle\phi_1^2\rangle} \quad (5)$$

The brackets here denote an ensemble average, and the phases ϕ_i are obtained as

$$\phi_i(t_a, t_b) = D_{eff}\int_{t_a}^{t_b} P_2(\cos\beta_t)\, dt \quad (6)$$

where the interval $t_b - t_a = \tau_{DQ}$, and the index $i = 1, 2$ denotes the excitation or reconversion period, respectively. In deriving the above relations, we closely follow BCS[21] and our previous work on the MQ NMR study of chain dynamics in elastomers.[24] The β echo of BCS is formally equivalent to the DQ buildup function, eq 3, and a discussion of differences due to the actual pulse sequence implementation is given in the preceding paper.[17] For completeness, we also include the expression for a Hahn echo of total duration τ_{echo}

$$I_{echo} = \left\langle \cos\frac{3}{2}\phi_{echo} \right\rangle \simeq e^{-(9/8)\langle\phi_{echo}^2\rangle} \quad (7)$$

where $\phi_{echo} = \phi(0,\tau_{echo})$. The additional factor of 3/2 marks the only formal difference between free homonuclear dipolar evolution and evolution under a DQ Hamiltonian, eq 2.

dx.doi.org/10.1021/ma102571u |*Macromolecules* 2011, 44, 1560–1569

The approximative solutions given in eqs 3−5 and 7 are based on the second-moment (AW) approximation,[19] which takes its main justification from the quasi-Gaussian frequency distribution in a powder sample. We stress that the above treatment is essentially a single-interaction (spin-pair) treatment, yet by virtue of the second-moment approximation, $D_{\mathrm{eff}} \sim M_{2\mathrm{eff}}^{1/2}$ takes the role of an effective quantity related to the dipolar second moment, which effectively represents the action of multiple dipole−dipole couplings. It must, however, be stressed that the approximation cannot be expected to properly describe the long-time behavior, as becomes immediately apparent by comparing single-interaction signal functions and the corresponding second-moment approximations (see Figures 5 and 6 of ref 18). In the static limit, about 80% of the initial intensity buildup (or decay) is well represented. Second-moment approximations usually fit an even larger data range in multiply coupled ^{1}H systems, yet the limit is rather strict when applied for instance to ^{2}H quadrupolar NMR.

An actual test of the validity range of the AW approximation, based exclusively on experimental data, is provided by the simple identity

$$I_{\mathrm{echo}}(\tau) = [I_{\Sigma\mathrm{MQ}}(\tau)(I_{\Sigma\mathrm{MQ}}(\tau) - 2I_{\mathrm{DQ}}(\tau))]^{9/16} \qquad (8)$$

which is easily proven by combining eqs 3, 5, and 7, identifying τ with either τ_{DQ} or τ_{echo}. This relation was previously tested on the example of signal functions of elastomers.[24]

Continuing with the AW expressions, the ensemble and time average is now to be taken over products of the individual phases, which is a rather straightforward exercise,[21,25] resulting in simple time integrals over the OACF, eq 1, namely

$$\langle \phi(0,\tau)^2 \rangle = \frac{4}{9} M_{2\mathrm{eff}} \times 2 \int_0^\tau (\tau - t')C(t')\, \mathrm{d}t' \qquad (9)$$

and

$$\langle \phi(0,\tau)\phi(\tau,2\tau) \rangle = \frac{4}{9} M_{2\mathrm{eff}} \left[\int_0^\tau t' C(t')\, \mathrm{d}t' + \int_\tau^{2\tau} (2\tau - t')C(t')\, \mathrm{d}t' \right] \qquad (10)$$

where $\phi(0,\tau) \equiv \phi_1$ or ϕ_{echo} and $\phi(\tau,2\tau) \equiv \phi_2$ as used above. We use a normalized OACF, $C(t{=}0) = 1$, and the common definition of the second moment, $M_{2\mathrm{eff}} = (9/20)D_{\mathrm{eff}}^2$, requiring the 4/9 correction factor due to the dipolar phase $\phi(0,\tau)$ representing evolution under a DQ pulse reference rather than free dipolar evolution.

III. RESULTS AND DISCUSSION

This section is organized as follows. We first present our *ansatz* for $C(t)$, which is based on purely experimental findings on linear polymers over a large molecular-weight (M) range, and calculate the NMR signal functions. Second, within the given theoretical framework, we address the validity and perspectives for the initial-rise approximation used in the analysis of MQ data to obtain $C(t)$ by time−temperature superposition.[14−17] Third, we compare the theoretical signal functions with data from MQ and Hahn echo experiments, and finally, we comment on previous related NMR approaches. Experimental details on the MQ data discussed herein, taken on a low-field instrument, can be taken from refs 16 and 17. Hahn echo data were acquired under the same experimental conditions for the same samples using a simple time-incremented $90_x-(\tau/2)-180_{\pm x}-(\tau/2)-$acquire pulse sequence.

3.1. Experimental OACF and Theoretical Signal Functions.

A schematic correlation function, based on previous work of Rössler and co-workers by field-cycling T_1 relaxatometry[13] and of us by MQ NMR,[16,17] is shown in Figure 1. See the latter references for an in-depth discussion of the scaling exponents and regime transition times, which are M-independent below and M-dependent above the entanglement time τ_{e}. In Figure 2, OACFs for three specific M of nearly monodisperse poly(butadiene) samples (PB) are shown along with experimental data.

We here seek an approximate analytical representation of $C(t)$, based on the dynamic regimes of the tube/reptation model. Note that the M-dependence of the regime II scaling exponent ε is not compatible with the latter model, so our regime classification should not be taken as a statement in full support of this model. The form of $C(t)$ that is compatible with the data, constructed in a piecewise fashion as connected power laws for regimes I−III and using the analytical result for regimes III and IV of BCS, reads

regime 0: $t < \tau_{\mathrm{s}}$

$$C_0 = A_0 + B\mathrm{e}^{-b\,t/\tau_{\mathrm{s}}} + C\mathrm{e}^{-c\,t/\tau_{\mathrm{s}}} \qquad (11)$$

regime I: $\tau_{\mathrm{s}} < t < \tau_{\mathrm{e}}$

$$C_{\mathrm{I}} = f\left(\frac{\tau_{\mathrm{s}}}{t}\right)^{0.85} \qquad (12)$$

regime II: $\tau_{\mathrm{e}} < t < \tau_{\mathrm{R}}$

$$C_{\mathrm{II}} = f\left(\frac{\tau_{\mathrm{s}}}{\tau_{\mathrm{e}}}\right)^{0.85}\left(\frac{\tau_{\mathrm{e}}}{t}\right)^{\varepsilon} \qquad (13)$$

regimes III and IV: $\tau_{\mathrm{R}} < t$

$$C_{\mathrm{III,IV}} = f\left(\frac{\tau_{\mathrm{s}}}{\tau_{\mathrm{e}}}\right)^{0.85}\left(\frac{\tau_{\mathrm{e}}}{\tau_{\mathrm{R}}}\right)^{\varepsilon}\left(\frac{\tau_{\mathrm{R}}}{t}\right)^{0.5} \sum_{p\ \mathrm{odd}} \frac{8}{p^2\pi^2}\mathrm{e}^{-p^2 t/\tau_{\mathrm{d}}} \qquad (14)$$

where $f = A_0 + B\mathrm{e}^{-b} + C\mathrm{e}^{-c}$. The regime transition times τ_x are defined in the caption of Figure 1. While the perfect complementarity of the combined field-cycling and MQ NMR data was already discussed in ref 16, we here note that for a truly quantitative match we had to scale down the MQ NMR data by a factor of 0.7 (see the inset in Figure 2). This indicates the shortcomings of our crude model for the absolute-value determination of $C(t)$, discussed in ref 17. The correction is almost equal to the factor of 0.75 observed upon isotopic dilution of a protonated homopolymer in 75% of its deuterated analogue,[16] suggesting that interchain dipole−dipole couplings may be the origin of the problem. Simply, our model for the reference coupling of a statistical segment D_{stat}/k needed to set the absolute value of $C(t)$ (see also ref 26) is based upon an isolated chain segment and does not take interchain couplings into account, while the latter of course contribute to the experimental data to some degree in both cases. Note that the "switching off" of interchain couplings by isotopic dilution did not lead to perceptible changes in the shape of $C(t)$ in regimes II−IV, yet changes in regimes 0 and I would not be unexpected,[27] providing a

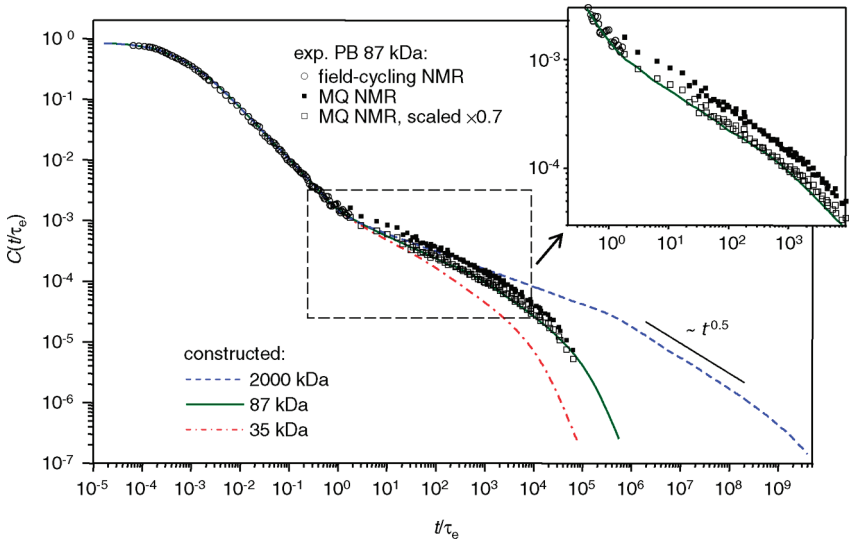

Figure 2. Segmental OACF for three different molecular weights of PB based on parameters listed in Table 1, including experimental data for the 87 kDa sample from field-cycling relaxometry[13] and MQ NMR.[16,17] To experimentally reach the reptation regime ($\sim t^{-1/2}$) on the time scale of MQ NMR (~1 ms) for the highest molecular weight, the measurements would have to be done at around 4000 K. The blow-up in the inset emphasizes the slight mismatch between the initial field-cycling and MQ NMR results.

Table 1. Experimentally Determined Parameters of $C(t)$ for PB from Refs 16 and 17 and Values of $D_{eff}/2\pi$ from Simultaneous Fits of I_{DQ} and $I_{\Sigma MQ}$ for the Data Sets Shown in Figure 4[a]

M_w [kDa]	ε	$\log(\tau_R/\tau_e)$	$\log(\tau_d/\tau_e)$	T [K]	$D_{eff}/2\pi$ [kHz]
35	0.43	1.9	4.1	273	17 ± 0.5
				343	16.5 ± 0.5
87	0.36	2.9	5.1	273	16.5 ± 0.5
				353	17.5 ± 0.5
441	0.31	4.1*	7.5*	273	16.0 ± 2.5
				353	16.0 ± 2.5
2000	0.29	5.4*	9.7*	273	15 ± 3
				363	14 ± 3

[a] The values denoted with asterisks (*) were not experimentally accessible and were thus extrapolated using the known power law for their M dependence (see Figure 8a of ref 17).

possible explanation for the −0.85 power law in regime I, where the Rouse-model prediction is −1. Herrmann et al. have ascribed their own observation to the limited number of Rouse modes in a finite and necessarily coarse-grained chain segment.[13]

The part describing regime 0 (glassy dynamics) requires a few additional comments. We attempted to fit the experimental data of Herrmann et al.[13] with as little as possible parameters, and the double exponential provided a sufficiently accurate representation of the data, with the parameters $A_0 = 0.0946$, $B = 0.457$, $b = 8.6$, $C = 0.449$, and $c = 1.45$. The numerical values are henceforth absorbed into the equations below. Note that using a constant factor $f = A_0 + Be^{-b} + Ce^{-c}$ for regimes I−IV means that we neglect further correlation loss due to subsegmental dynamics in these regimes. Either A_0 or f may be taken to represent apparent plateau values describing the residual orientation correlations within a Kuhn segment, $\sim C(\tau_s)$. The corresponding intrasegmental "order parameter" $S \approx (C(\tau_s))^{1/2}$ thus ranges between around 0.3 and 0.45. The influence of glassy dynamics on $C(t)$, or more generally on T_1 dispersion NMR data, has been the subject of papers of Rössler and co-workers.[28−30] Claiming a separability of subsegmental dynamics and chain modes on the basis of an additivity assumption in the "susceptibility representation" $\omega/T_1(\omega)$, they arrived at an equivalent order parameter. A clean separation would strictly require a short-time plateau value in $C(t)$, which is not visible in the $C(t)$ data obtained from $\omega/T_1(\omega)$ by Fourier transformation. However, the good agreement between the apparent value range given above and the higher-M value of from the latter approach, $S \approx 0.35$,[30] appears to support the concept.

Another potential problem in regime 0, also related to the simple calculation of $C(t)$ by Fourier transformation of $\omega/T_1(\omega)$, is that the latter more precisely depends on the spectral densities $j_1(\omega)$ and $j_2(2\omega)$, which are Fourier transformations of the autocorrelation functions of second-degree spherical harmonics or order 1 and 2, respectively. These reduce to the OACF of the second Legendre polynomial (order 0) only for uniaxially symmetric dynamics, which is not necessarily the case for the subsegmental α process at short times. Further, the ω and 2ω dependencies were equated, which is a small error on logarithmic scales, yet may lead to additional systematic errors in our representation of regime 0 dynamics.

In order to use eqs 3−5 and 7 to obtain signal functions, the remaining task is to evaluate the phase correlations via inserting the OACF defined in eqs 11−14 into eqs 9 and 10. This is straightforward for the evaluation of eq 9, which falls into four separate integrals at most, depending on the final time value τ:

$\tau < \tau_s$:

$$\langle\phi(0,\tau)^2\rangle_0 = \frac{8}{9}M_{2eff}[0.0407\tau^2 + (0.266\tau - 0.184\tau_s)\tau_s + (0.0457\tau - 0.00531\tau_s)\tau_s] + \frac{8}{9}M_{2eff}(0.00531e^{-8.6\tau/\tau_s} + 0.184e^{-1.45\tau/\tau_s})\tau_s^2 \quad (15)$$

dx.doi.org/10.1021/ma102571u |Macromolecules 2011, 44, 1560–1569

$\tau_s < \tau < \tau_e$:

$$\langle\phi(0,\tau)^2\rangle_{\mathrm{I}} = \frac{4}{9}M_{2\mathrm{eff}}(0.662\tau - 0.248\tau_s)\tau_s + \frac{4}{9}M_{2\mathrm{eff}}(1.995\tau^{1.15}{\tau_s}^{0.85} - 2.295\tau\tau_s + 0.299{\tau_s}^2) \quad (16)$$

$\tau_e < \tau < \tau_R$:

$$\langle\phi(0,\tau)^2\rangle_{\mathrm{II}} = \frac{\frac{4}{9}M_{2\mathrm{eff}}0.344(\tau^2{\tau_e}^{\varepsilon} + \tau^{\varepsilon+1}\tau_e(\varepsilon-2) + (1-\varepsilon)\tau^{\varepsilon}{\tau_e}^2){\tau_s}^{0.85}}{\tau^{\varepsilon}(\varepsilon-2)(\varepsilon-1)\tau_e e^{0.85}} + \frac{4}{9}M_{2\mathrm{eff}}[(0.662\tau - 0.248\tau_s)\tau_s + 2.295\tau({\tau_e}^{0.15}{\tau_s}^{0.85} - \tau_s) + 0.299({\tau_s}^2 - {\tau_e}^{1.15}{\tau_s}^{0.85})] \quad (17)$$

$\tau_R < \tau$:

$$\langle\phi(0,\tau)^2\rangle_{\mathrm{III,IV}} = \frac{4}{9}M_{2\mathrm{eff}} \times 0.344\frac{{\tau_s}^{0.85}}{{\tau_e}^{0.85}}\left(\frac{{\tau_e}^2 - {\tau_e}^{\varepsilon}{\tau_R}^{2-\varepsilon}}{2-\varepsilon} + \frac{\tau{\tau_R}^{-\varepsilon}({\tau_e}{\tau_R}^{\varepsilon} - {\tau_e}^{\varepsilon}\tau_R)}{\varepsilon - 1}\right) + \frac{4}{9}M_{2\mathrm{eff}}[(0.662\tau - 0.248\tau_s)\tau_e + 2.295\tau({\tau_e}^{0.15}{\tau_s}^{0.85} - \tau_s) + 0.299({\tau_s}^2 - {\tau_e}^{1.15}{\tau_s}^{0.85})] + \sum_{p\ \mathrm{odd}} \frac{\frac{4}{9}M_{2\mathrm{eff}} \times 1.377\left(\frac{\tau_e}{\tau_R}\right)^{\varepsilon}\sqrt{\tau_R{\tau_d}^3}\left(\frac{\tau_s}{\tau_e}\right)^{0.85}}{p^5\pi^2}$$

$$\times\{2(e^{-x\tau}\sqrt{x\tau} - e^{-x\tau_R}\sqrt{x\tau_R}) + \sqrt{\pi}(1-2x\tau)(\mathrm{erf}[\sqrt{x\tau_R}] - \mathrm{erf}[\sqrt{x\tau}])\} \quad (18)$$

with $x \equiv p^2/\tau_d$ and $\mathrm{erf}(y) = \int_{-\infty}^{y} e^{-q^2}\,dq$. The above piecewise $\langle\phi(0,\tau)^2\rangle$ can be immediately used to calculate the Hahn echo decay, eq 7. For the MQ signal functions, one needs to further evaluate eq 10, where the appearance of the 2τ term means that there are additional regime crossovers which have to be considered upon integration. We refrain from reporting the lengthy results and recommend the use of computer algebra software for handling such calculations. We restrict ourselves to just giving an illustrative example for the calculation details in the interval $^1/_2\tau_e < \tau < \tau_e$:

$$\langle\phi(0,\tau)\phi(\tau,2\tau)\rangle = \frac{4}{9}M_{2\mathrm{eff}}[\int_0^{\tau_s} t'C_{\mathrm{I}}(t')\,dt' + \int_{\tau_s}^{\tau} t'C_{\mathrm{I}}(t')\,dt' + \int_{\tau}^{\tau_e}(2\tau - t')C_{\mathrm{I}}(t')\,dt' + \int_{\tau_e}^{2\tau}(2\tau - t')C_{\mathrm{II}}(t')\,dt'] \quad (19)$$

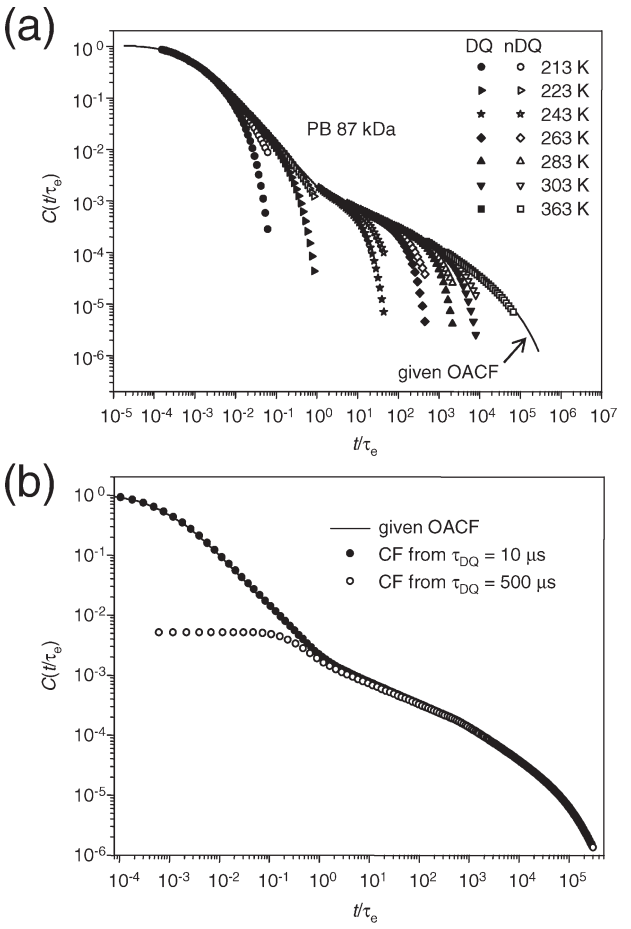

Figure 3. (a) Constructed correlation function for PB of 87 kDa (solid line, see Figure 2) serving as input for the theoretical treatment, and superposed analytical results for $I_{\mathrm{nDQ}}(\tau_{\mathrm{DQ}})/(k{\tau_{\mathrm{DQ}}}^2)$ and $I_{\mathrm{DQ}}(\tau_{\mathrm{DQ}})/(k{\tau_{\mathrm{DQ}}}^2)$ over a large range of nominal temperatures, converting τ_{DQ} to t/τ_e by division through $\tau_e(T)$ (TTS). (b) Reconstruction of the given OACF by single-point measurements of $I_{\mathrm{nDQ}}(\tau_{\mathrm{DQ}})$ for different fixed τ_{DQ} = 10 and 500 μs at many different different temperatures, scaled with a common prefactor $k{\tau_{\mathrm{DQ}}}^2$ and shifted along the time axis using TTS.

All calculations are generally based upon the molecular-weight dependent experimental values of ε, τ_R, and τ_d listed in Table 1 or upon suitably interpolated values. The temperature dependence of the monomeric friction coefficient $\xi(T)$ for PB can be taken from the literature,[31] and then τ_e is obtained according to $\tau_e = {N_e}^2\tau_s$ and $\tau_s = \xi(T)b^2/\pi k_B T$; see refs 16 and 17 for parameter values and a discussion on the relation between τ_s and the α relaxation time of glassy dynamics.

3.2. OACF As Obtained via Initial-Rise Analysis. With analytical solutions for all relevant NMR signal functions at hand, we first address the validity of our experimental approach to determine $C(t)$ by analyzing point-by-point normalized DQ (nDQ) buildup data, $I_{\mathrm{nDQ}} = I_{\mathrm{DQ}}/I_{\Sigma\mathrm{MQ}}$, in the short-time regime.[16,17] It was already shown by Graf et al.[14,15] that for short τ_{DQ} the nDQ intensity is proportional to $C(\tau_{\mathrm{DQ}})$

$$I_{\mathrm{nDQ}}(\tau_{\mathrm{DQ}}) \approx k{\tau_{\mathrm{DQ}}}^2 C(\tau_{\mathrm{DQ}}) \quad (20)$$

By changing the temperature, which leads to known changes in $\tau_e(T)$, master curves for $C(t/\tau_e) \sim I_{n\mathrm{DQ}}(\tau_{\mathrm{DQ}})/{\tau_{\mathrm{DQ}}}^2$ can thus be

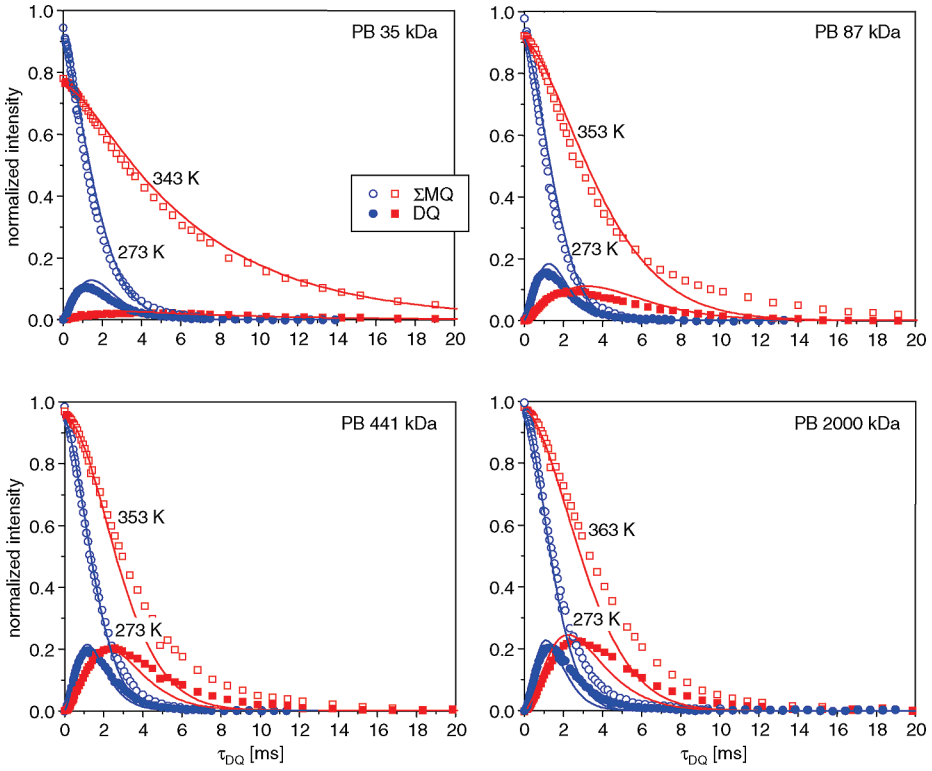

Figure 4. Experimental I_{DQ} and $I_{\Sigma MQ}$ data of PB at two different temperatures and for different molecular weights: 35, 87, 441, and 2000 kDa. The solid lines represent analytical predictions, with parameters given in Table 1. $M_{2eff} = (9/20)D_{eff}^2$ was taken constant using the average $D_{eff}/2\pi = 16$ kHz. Note that the overall intensity scale refers to unity as the full sample magnetization, and $I_{\Sigma MQ}(0)$ represents the signal associated with chain-center segments after subtraction of sample- and temperature-dependent signal tails related to isotropically mobile chain ends and loops.[17]

constructed by time−temperature superposition (TTS). While the accessible time range is rather narrow, making it difficult to confirm the validity of TTS by acquiring data with sufficient overlap, we note that at a given temperature the scaling exponent (slope of $C(t)$ vs t in a log−log plot) can be determined with acceptable accuracy at a given temperature from the initial rise of $I_{nDQ}(\tau_{DQ})$, confirming at least the qualitative features of $C(t)$ independent of TTS (see our previous paper[17]).

In previous work, the TTS-based analysis was restricted to regime II dynamics with $\tau_{DQ} > \tau_e$, based on the notion that relaxation effects due to faster segmental dynamics in regimes 0 and I, which are known to mainly affect $I_{\Sigma MQ}$ (and thus also the long-time decay of I_{DQ}), are divided out by nDQ calculation. This increases the validity range of the initial-rise approximation. The sensitivity of $I_{\Sigma MQ}$ mainly to fast dynamics was demonstrated in ref 24 (see also Figure 4). The underlying assumptions are also proven by the fact that I_{nDQ} is independent of temperature for elastomers at sufficiently high temperature, where $C(t)$ has a plateau due to the absence of terminal dynamics.[18]

We can now address the limitations of this approach, including the question whether the segmental dynamics really has to be fast on the τ_{DQ} time scale in order to validate the intensity normalization and the use of eq 20. In Figure 3a we compare the given experiment-based $C(t)$ with adequately processed analytical signal functions. Obviously, $C(t)$ is indeed obtained as the exact envelope provided by individual nDQ buildup curves (see also Figure 7 of ref 17). We confirm that the intensity normalization leads to an increased validity range of the fit, but we can also note that it is not strictly necessary—also, the I_{DQ} data provide a good measure of $C(t)$, of course over a shorter time range.

Even more interestingly, it is seen that it should be equally possible to extend the advantageous time-domain probe of $C(t)$ via initial-rise analysis also to regimes 0 and I. Corresponding experiments are in progress, but we stress that the need to access rather short τ_{DQ} requires the use of a different MQ pulse sequence, namely, a simple 2- or 3-pulse segment rather than our commonly used multipulse sequence.[18] The latter is limited to τ_{DQ} longer than ∼60 μs, and its efficiency breaks down once the apparent residual dipole−dipole couplings in the system, proportional to $[C(t \approx \tau_{DQ})]^{1/2}$, are too high.

The latter limitations are technical, related to the validity of the average Hamiltonian given by eq 2, but corresponding arguments can be made with respect to the general validity of the initial-rise approximation, eq 20, which also breaks down at a certain maximum τ_{DQ}. The validity range depends on the magnitude of $C(\tau_{DQ})$, and thus, probing $C(t)$ at low temperatures, thus short times t, requires the use of short τ_{DQ}. This is addressed in Figure 3b for two different values of τ_{DQ}, the lower value of 10 μs being only accessible with the simple 2- or 3-pulse MQ experiment or, in fact, also the β echo.[20] Evaluating I_{nDQ} only at fixed single-time points was in fact one of the limitations of the earliest approach by Graf et al.,[14,15] who used a magic-angle spinning sequence with a long cycle time fixed to two rotor periods. Obviously, the longer the fixed τ_{DQ}, the earlier one observes deviations from the expected $C(t)$ upon decreasing the temperature. Fortunately, even at 500 μs evolution time, strong deviations are only apparent around and below τ_e.

3.3. Prediction of Experimental Signal Functions. The $I_{\Sigma MQ}$ and in particular the I_{DQ} signal functions measured for PB as plotted in Figure 4 are rather sensitive to changes in

dx.doi.org/10.1021/ma102571u |*Macromolecules* 2011, 44, 1560–1569

temperature and molecular weight. The strong increase of the intensity of the DQ signal with M is a clear signature of the increased number of entanglements, while its temperature dependence additionally reflects the chain dynamics in regimes II−IV. We also confirm that in the higher M range $I_{\Sigma MQ}$ is not much dependent on M, indicating that this observable mainly reflects dynamics in regimes 0 and I.

Using the parameters given in Table 1 and the $\tau_{s,e}(T)$ given in ref 17, analytical predictions of this data require the determination of only one parameter, namely $M_{2eff} = (9/20)D_{eff}^2$. We performed simultaneous fits to both data sets for a given sample and temperature, obtaining values ranging around $D_{eff}/2\pi = 16 \pm 1$ kHz (see also Table 1). In the investigate M range, we observe a weak systematic trend of somewhat lower D_{eff} toward higher M, while a constant value would be expected.

The average result of $D_{eff}/2\pi = 16 \pm 1$ kHz for the effective coupling constant may be compared to the considerably lower intrasegmental reference value of 8.1 kHz from our previous simulations.[26] This trend is expected, as D_{eff} should represent the rigid system as reference state subject to α relaxation and all slower modes (i.e., $[C(t \ll \tau_\alpha)]^{1/2}$), while our reference value represents a Kuhn segment containing several monomers exhibiting a certain degree of conformational dynamics (i.e., $[C(t=\tau_s)]^{1/2}$).

On the other hand, the present result is somewhat smaller than values of around 23 ± 5 kHz calculated from rigid-limit intramolecular second moments for PB estimated for a variety of structural models.[32] Overall, it falls into a reasonable range, considering the uncertainties discussed above in relation to the exact form of $C(t)$ in regime 0. These may further be aggravated by a possible influence of faster β processes and general problems related to the failure of time−temperature superposition for temperatures close to T_g.[33] The weak systematic decrease with M could further be due to parameter interdependencies related to the M-dependent shape of $C(t)$ at longer times, where our representation by a sequence of power laws is still to some degree approximate.

In all, the analytical predictions shown in Figure 4 demonstrate a very satisfactory agreement between the theoretical approach and actual data for the rather wide sample and temperature range covered. We note that using the individual best-fit D_{eff} instead of the global average provides visibly even better fits.

Finally in Figure 5, we present Hahn echo (T_2) decay curves for the two samples at the extremes of the M interval and for the same temperatures as in Figure 4. Again, the agreement of the data with the analytical predictions is very good in the expected range covering the greater part of the intensity decay. We thus conclude that the present approach for the calculation of transverse relaxation phenomena, being based on the AW approximation and a realistic, experiment-based and phenomenologically realistic model function for the segmental orientation fluctuations, represents a significant step forward over the many alternative treatments published so far.

3.4. Relation to and Critical Discussion of Previous NMR Work. For a good overview of NMR observables of polymer dynamics, we refer the reader to a recent review of Kimmich and Fatkullin,[10] which has its emphasis on field-cycling T_1 relaxometry. Alternative interpretations of such results have recently been proposed by Rössler and co-workers,[13,28−30] whose data provided the short-time region of our composite $C(t)$.

The MQ method has a rather long history, in particular as to employing the special properties of the nDQ buildup function in

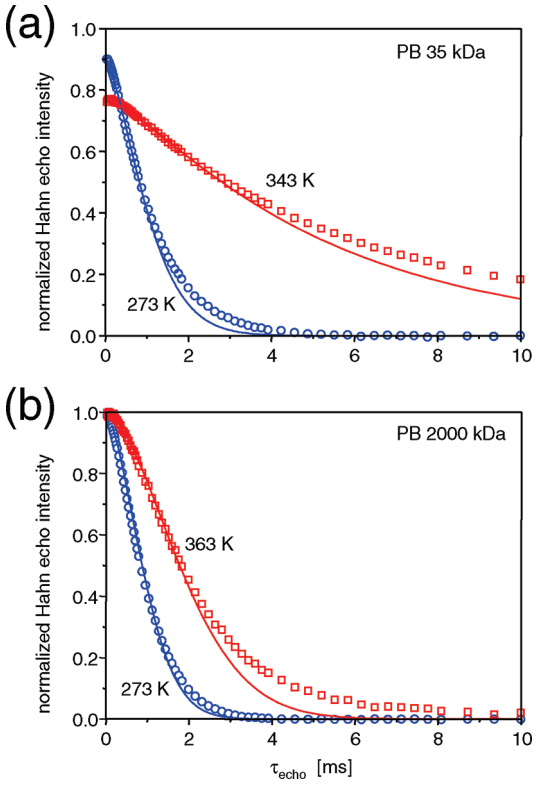

Figure 5. Experimental Hahn echo data of PB as a function of temperature and molecular weight: (a) 2000 and (b) 35 kDa. Solid lines represent the predictions without adjustable parameters, using the same parameters and the same M_{2eff} values as for the data in Figure 4. Small contributions of slowly relaxing signal tails related to isotropically mobile segments were again subtracted.

studying entangled melt dynamics. Cohen-Addad was the first to establish a specific combination of Hahn and solid echo pulse sequence elements to obtain a shift-compensated build-up function providing a measure of residual dipole−dipole couplings.[34,35] At this early point, the residual couplings in highly entangled melts were assumed to be quasi-static. Spiess and co-workers later pointed out that using Anderson−Weiss type arguments for the analysis of similar experimental data, assuming a single-exponential correlation function describing a decay of the orientation correlations at longer times, can give a better description of the data. This was assumed to reflect the effect of finite entanglement lifetime, however, without establishing relations to the common time scales of chain motion.[36] Later, Kimmich and co-workers established the dipolar correlation effect on the stimulated echo as a means to study slower chain motions with better sensitivity[37] but could only state that the long-time correlation loss is best described by a power law with an exponent of around −3/2. This result in fact agrees with the tube-model prediction at around τ_d (see Figure 1b of ref 17).

BCS were the first to present the β echo[20] as an experiment providing a clean sine−sine buildup function corresponding to eq 3 and to use it for the study of melt dynamics in the framework of a closed-form Anderson−Weiss theory based on an OACF inspired by the tube model.[21,22] Their assumption was to neglect fast regime 0, I dynamics, so their modeling started at the level of the entanglement-induced chain order ($C(t \leq \tau_e) = cst \ll 1$), assuming a fixed −1/4 power law for regime II and the same form as discussed above for regimes III and IV. Their fits gave a fair

agreement of the fitted terminal time to an M^3 dependence, yet good fits to data could only be reported for large molecular weights exceeding 30 entangled units. Cohen-Addad later presented a refined analysis of his early experimental approach,[38] deriving a quantity related to the terminal time, exhibiting a $M^{3.3}$ power law dependence, in agreement with our findings, and attributing the 0.3 deviation to M-dependent segmental friction.

In a more recent paper, Chernov and Krasnopol'skii combined the analysis of different relaxation times (T_1, T_2, and $T_{2\mathrm{eff}}$ from a solid-echo type sequence), measured separately at low field, to derive a schematic OACF that now also included the fast (regime 0, I) branch.[39] They concluded satisfactory agreement of the features of their OACF with the Doi−Edwards prediction in regimes II−IV but also pointed out that their data are only consistent with a regime I slope of about −0.8, being smaller than the Rouse prediction (−1), as confirmed by the field-cycling data of Rössler.[13] Our direct time-domain measure of $C(t)$ based on MQ NMR, first introduced by Spiess and co-workers[14,15] but in the earlier variant subject to some limitations discussed above and in refs 16 and 17, finally confirmed important deviations from the tube-model predictions with respect to the protracted onset of actual reptation and a molecular-weight-dependent regime II exponent ε.

With the current work, we have shown that the so-obtained $C(t)$, combined with Fourier-transformed field-cycling T_1 data, provides a consistent description of the actual chain dynamics over about 10 decades in time and serves as a sound basis for an Anderson−Weiss prediction of the signal functions that are in good agreement with actual MQ and Hahn-echo data. Our results immediately disprove a conclusion of Brereton,[40] stating that "The well-known second moment approximation is shown to be seriously wrong when the time scale of the bond dynamics is comparable or greater than the NMR time scale set by the dipolar interactions."

Brereton's approach, consisting in a path-integral based "exact" calculation of the dipolar dephasing (Hahn echo) function $\langle \cos \phi(0,\tau) \rangle$ for a scale-invariant Gaussian chain model,[40−42] has proven well-applicable in the unentangled (Rouse) limit.[43,44] In this regime, the underlying model appears indeed exact in a sense that the chain motion reaches the isotropic limit on time scales shorter than the actual Hahn echo decay, and in this region, the relaxation function is single exponential. In the latter references, good fits to actual data for well-entangled polymers could not be reported, mainly due to the lack of sufficient short-time data points (which are most meaningful) and the lack of a proper model describing entangled dynamics. Analyzing a suitably extracted global T_2 parameter on the basis of a single-relaxation time model describing terminal dynamics provided the expected $M^{3.5}$ dependence, yet the question remains why Brereton's model appears to encounter fundamental problems with well-entangled chains or networks.

We have addressed this question for the example of permanent elastomers,[45] where $C(t)$ has a long-time plateau (absence of any slow processes) after an initial decay that we could show to be also best described by a power law with an exponent in the range between −1 and −0.6.[24] At sufficiently high temperatures, when the chain modes are in the fast limit, the normalized DQ buildup is completely temperature-independent and only reflects residual dipole−dipole couplings arising from the network constraint.[18] While many elastomers exhibit a response that can be perfectly fitted with a single apparent residual coupling based on a second-moment function,[18] Brereton's model yields a function that is equivalent to alternative calculations based a broad Gamma distribution of couplings.[42,45] This distribution ultimately arises from a model-inherent assumption of a (quasi-)frozen end-to-end vector distribution, including for instance chains that exhibit very small end-to-end distances and are thus characterized by very small residual couplings. While some defect-rich networks do show such a response (corresponding to what is sometimes called a "super-Lorentzian" line shape), it is not generic—network constraints are generally rather homogeneous,[45] possibly due to locally balanced entropic forces[46] and because loop structures with close end points are likely to be topologically constrained. The latter naturally holds for properly modeled entanglement constraints, arising for instance from a tube theory. The recently suggested extension of the Brereton theory to MQ signal functions,[47] being again based on a single-relaxation time model, is thus unfortunately not expected to yield meaningful results for real polymer chains.

IV. CONCLUSIONS

We have shown that based on our previously derived segmental orientation correlation function for entangled polymers, covering the regimes inspired by the Doi−Edwards tube model including "glassy" short-time intrasegmental dynamics, it is possible to derive analytical expressions for NMR time-domain signals on the basis of the Anderson−Weiss approximation. These are demonstrated to be in very good agreement with data from Hahn echo and multiple-quantum experiments over a large temperature and molecular weight range, establishing for the first time a consistent theoretical description of NMR data based on a generic description of the chain dynamics covering more than 10 decades in time.

Future perspectives arising from our present theoretical considerations include the application of our time-domain measure of the correlation function at lower temperatures, thus directly probing the dynamics in regime 0 and I. Further, we are currently testing the evaluation of reliable fitting procedures, based on simultaneous fits of different signal functions, that should yield scaling exponents and characteristic times at a given temperature without relying on time−temperature superposition. These efforts will benefit from a better understanding and modeling of the intrasegmental dynamics, where also chemically realistic computer simulations will help. In addition, current theoretical efforts are focused on a chain-based Rouse-type model for $C(t)$, implementing different approaches to take into account orientation correlations, such as fixed ends (describing elastomers), homogeneously distributed slip- or slide-links, or a homogeneous confining potential, thus being able to implement and test modern realizations of tube constraints.

AUTHOR INFORMATION

Corresponding Author

*E-mail: (K.S.) kay.saalwaechter@physik.uni-halle.de; (F.V.C.) fvchavez@cii.fc.ul.pt.

Present Addresses

[†]Centro de Física da Matéria Condensada Universidade de Lisboa, Lisbon, Portugal.

ACKNOWLEDGMENT

Funding of this work was provided by the Deutsche Forschungsgemeinschaft (SA 982/3-1). We thank S. Stepanow for

his theoretical advice, R. Kimmich and N. Fatkullin for critical comments and stimulating discussions, and Marie Lehnich for supplying the Hahn echo data in Figure 5. Infrastructure support from the European Union (ERDF programme) is gratefully acknowledged.

REFERENCES

(1) de Gennes, P. G. Reptation of a Polymer Chain in the Presence of Fixed Obstacles. *J. Chem. Phys.* **1971**, *55*, 572–579.

(2) Rouse, P. E., Jr. A Theory of the Linear Viscoelastic Properties of Dilute Solutions of Coiling Polymers. *J. Chem. Phys.* **1953**, *21*, 1272–1280.

(3) Doi, M.; Edwards, S. F. *The Theory of Polymer Dynamics*; Clarendon Press: Oxford, 1986.

(4) McLeish, T. C. B. Tube theory of entangled polymer dynamics. *Adv. Phys.* **2002**, *51*, 1379–1527.

(5) Ferry, J. D. *Viscoelastic Properties of Polymers*; John Wiley: New York, 1980.

(6) Kremer, F., Schönhals, A., Eds. *Broadband Dielectric Spectroscopy*; Springer: Berlin, 2003.

(7) Roe, R.-J. *Methods of X-Ray and Neutron Scattering in Polymer Science*; Oxford University Press: Oxford, 2000.

(8) Strobl, G. *The Physics of Polymers*, 3rd revised ed.; Springer: Berlin, 2007.

(9) Schmidt-Rohr, K.; Spiess, H. W. *Multidimensional Solid-State NMR and Polymers*; Academic Press: London, 1994.

(10) Kimmich, R.; Fatkullin, N. Polymer chain dynamics and NMR. *Adv. Polym. Sci.* **2004**, *170*, 1–113.

(11) Kreer, T.; Baschnagel, J.; Müller, M.; Binder., K. Monte Carlo Simulations of Long Chain Polymer Melts: Crossover from Rouse to Reptation Dynamics. *Macromolecules* **2001**, *34*, 1105–1117.

(12) Stephanou, P. S.; Baig, C.; Tsolou, G.; Mavrantzas, V. G.; Kröger, M. Quantifying chain reptation in entangled polymer melts: Topological and dynamical mapping of atomistic simulation results onto the tube model. *J. Chem. Phys.* **2010**, *132*, 124904.

(13) Herrmann, A.; Novikov, V. N.; Rössler, E. A. Dipolar and Bond Vector Correlation Function of Linear Polymers Revealed by Field Cycling ^{1}H NMR: Crossover from Rouse to Entanglement Regime. *Macromolecules* **2009**, *42*, 2063–2068.

(14) Graf, R.; Heuer, A.; Spiess., H. W. Chain-Order Effects in Polymer Melts Probed by ^{1}H Double-Quantum NMR Spectrocopy. *Phys. Rev. Lett.* **1998**, *80*, 5738–5741.

(15) Dollase, T.; Graf, R.; Heuer, A.; Spiess, H. W. Local Order and Chain Dynamics in Molten Polymer-Blocks Revealed by Proton Double-Quantum NMR. *Macromolecules* **2001**, *34*, 298–309.

(16) Vaca Chávez, F.; Saalwächter., K. NMR Observation of Entangled Polymer Dynamics: Tube Model Predictions and Constraint Release. *Phys. Rev. Lett.* **2010**, *104*, 198305.

(17) Vaca Chávez, F.; Saalwächter, K. Time-domain NMR observation of entangled polymer dynamics: Universal behavior of flexible homopolymers and applicability of the tube model. *Macromolecules* **2011**, DOI: 10.1021/ma1025708.

(18) Saalwächter, K. Proton Multiple-Quantum NMR for the Study of Chain Dynamics and Structural Constraints in Polymeric Soft Materials. *Progr. NMR Spectrosc.* **2007**, *51*, 1–35.

(19) Anderson, P. W.; Weiss, P. R. Exchange Narrowing in Paramagnetic Resonance. *Rev. Mod. Phys.* **1953**, *25*, 269–276.

(20) Callaghan, P. T.; Samulski, E. T. Molecular Ordering and the Direct Measurement of Weak Proton−Proton Dipolar Interactions in a Rubber Network. *Macromolecules* **1997**, *30*, 113–122.

(21) Ball, R. C.; Callaghan, P. T.; Samulski., E. T. A simplified approach to the interpretation of nuclear spin correlations in entangled polymeric liquids. *J. Chem. Phys.* **1997**, *106*, 7352–7361.

(22) Callaghan, P. T.; Samulski., E. T. The Molecular Weight Dependence of Nuclear Spin Correlations in Entangled Polymeric Liquids. *Macromolecules* **1998**, *31*, 3693–3705.

(23) Baum, J.; Pines, A. Multiple-Quantum NMR Studies of Clustering in Solids. *J. Am. Chem. Soc.* **1986**, *108*, 7447–7454.

(24) Saalwächter, K.; Heuer., A. Chain Dynamics in Elastomers as Investigated by Proton Multiple-Quantum NMR. *Macromolecules* **2006**, *39*, 3291–3303.

(25) Kimmich, R. *NMR Tomography, Diffusometry, Relaxometry*; Springer: Berlin, 1997.

(26) Saalwächter, K.; Herrero, B.; López-Manchado, M. A. Chain order and crosslink density of elastomers as investigated by proton multiple-quantum NMR. *Macromolecules* **2005**, *38*, 9650–9660.

(27) Fatkullin, N.; Gubaidullin, A.; Stapf, S. Features of polymer chain dynamics as revealed by intermolecular nuclear magnetic dipole-dipole interaction: Model calculations and field-cycling NMR relaxometry. *J. Chem. Phys.* **2010**, *132*, 094903.

(28) Kariyo, S.; Gainaru, C.; Schick, H.; Brodin, A.; Novikov, V. N.; Rössler, E. A. From a Simple Liquid to a Polymer Melt: NMR Relaxometry Study of Polybutadiene. *Phys. Rev. Lett.* **2006**, *97*, 207803.

(29) Kariyo, S.; Brodin, A.; Gainaru, C.; Herrmann, A.; Schick, H.; Novikov, V. N.; Rössler., E. A. From Simple Liquid to Polymer Melt. Glassy and Polymer Dynamics Studied by Fast Field Cycling NMR Relaxometry: Low and High Molecular Weight Limit. *Macromolecules* **2008**, *41*, 5313–5321.

(30) Kariyo, S.; Brodin, A.; Gainaru, C.; Herrmann, A.; Hintermeyer, J.; Schick, H.; Novikov, V. N.; Rössler., E. A. From Simple Liquid to Polymer Melt. Glassy and Polymer Dynamics Studied by Fast Field Cycling NMR Relaxometry: Rouse Regime. *Macromolecules* **2008**, *41*, 5322–5332.

(31) Klopffer, M.-H.; Bokobza, L.; Monnerie, L. Effect of vinyl content on the viscoelastic properties of polybutadienes and polyisoprenes − monomeric friction coefficient. *Polymer* **1998**, *39*, 3445–3449.

(32) Sergeev, N. M.; Karpov, V. L. Calculation of the Intramolecular Second Moment of Proton Resonance Absorption Lines in Polybutadienes. *J. Mol. Struct.* **1965**, *5*, 208–212.

(33) Sokolov, A. P.; Schweizer, K. S. Resolving the Mystery of the Chain Friction Mechanism in Polymer Liquids. *Phys. Rev. Lett.* **2009**, *102*, 248301.

(34) Cohen-Addad, J. P.; Vogin, R. Molecular Motion Anisotropy as Reflected by a Pseudosolid" Nuclear Spin Echo: Observation of Chain Constraints in Molten *cis*-1,4,-Polybutadiene. *Phys. Rev. Lett.* **1974**, *33*, 940–943.

(35) Cohen-Addad, J. P. Method of measurement of nonzero average dipolar spin coupling in molten polymers. *J. Chem. Phys.* **1975**, *63*, 4880–4885.

(36) Collignon, J.; Sillescu, H.; Spiess, H. W. Pseudo-solid echoes of proton and deuteron NMR in polyethylene melts. *Colloid Polym. Sci.* **1981**, *259*, 220–226.

(37) Kimmich, R.; Fischer, E.; Callaghan, P.; Fatkullin., N. The Dipolar-Correlation Effect on the Stimulated Echo. Application to Polymer Melts. *J. Magn. Reson.* **1995**, *117*, 53–61.

(38) Cohen Addad, J.-P.; Guillermo., A. NMR and Entangled Chain Dynamics in Molten Polybutadiene. Molecular Weight Dependent Segmental Friction. *Macromolecules* **2003**, *36*, 1609–1615.

(39) Chernov, V. M.; Krasnopol'skii, G. S. Nuclear Magnetic Relaxation, Correlation Time Spectrum, and Molecular Dynamics in a Linear Polymer. *J. Exp. Theor. Phys.* **2008**, *107*, 354–366.

(40) Brereton, M. G. An exact expression for the transverse nuclear magnetic resoance relaxation of a dynamic scale invariant polymer chain governed by a single relaxation time. *J. Chem. Phys.* **1991**, *94*, 2136–2142.

(41) Brereton., M. G. NMR Transverse Relaxation Function Calculated for the Rouse Model. *Macromolecules* **1989**, *22*, 3667–3674.

(42) Brereton., M. G.; Transverse, N. M. R. Relaxation Function Calculated for Constrained Polymer Chains: Application to Entanglements and Networks. *Macromolecules* **1990**, *23*, 1119–1131.

(43) Brereton, M. G.; Ward, I. M.; Boden, N.; Wright, P. Nature of Proton NMR Transverse Relaxation Function of Polyethylene Melts. 1. Monodispersed Polyethylenes. *Macromolecules* **1991**, *24*, 2068–2074.

(44) Klein, P. G.; Adams, C. H.; Brereton, M. G.; Ries, M. E.; Nicholson, T. M.; Hutchings, L. R.; Richards., R. W. Rouse and Reptation Dynamics of Linear Polybutadiene Chains Studies by ^{2}H NMR Transverse Relaxation. *Macromolecules* **1998**, *31*, 8871–8877.

(45) Saalwächter, K.; Sommer., J.-U. NMR Reveals Non-Distributed and Uniform Character of Network Chain Dynamics. *Macromol. Rapid Commun.* **2007**, *28*, 1455–1465.

(46) Sommer, J.-U.; Chassé, W.; Valentín, J. L.; Saalwächter, K. Effect of excluded volume on segmental orientation correlations in polymer chains. *Phys. Rev. E* **2008**, *78*, 051803.

(47) Ries, M. E.; Brereton, M. G. An analytic expression for the double quantum ^{1}H nuclear magnetic resonance build-up and decay from a Gaussian polymer chain with dynamics governed by a single relaxation time. *Phys. Chem. Chem. Phys.* **2009**, *11*, 6918–6924.